Hindawi
International Transactions on Electrical Energy Systems
Volume 2022, Article ID 3714475, 16 pages
https://doi.org/10.1155/2022/3714475

Research Article

Developing a Marine Predator Algorithm for Optimal Power Flow Analysis considering Uncertainty of Renewable Energy Sources

Mohamed Farhat,[1] **Salah Kamel**,[2] **Ahmed M. Atallah**,[1] **and Baseem Khan**[3]

[1]*Electrical Power and Machines Engineering Department, Faculty of Engineering, Ain Shams University, Cairo 11517, Egypt*
[2]*Department of Electrical Engineering, Faculty of Engineering, Aswan University, Aswan 81542, Egypt*
[3]*Department of Electrical Engineering, Hawassa University, Awasa, Ethiopia*

Correspondence should be addressed to Salah Kamel; skamel@aswu.edu.eg

Received 25 December 2021; Revised 25 March 2022; Accepted 22 April 2022; Published 1 June 2022

Academic Editor: Kin Cheong Sou

Optimal power flow (OPF) is a crucial issue to maintain the reliable operation of power systems. However, achieving this objective is not easy, especially when renewable energy sources (RESs) are penetrated into the power system due to their uncertainty nature. This paper provides an optimal solution for the power flow problem including two different types of RESs based on a marine predator algorithm (MPA). The OPF model used in this paper has three different types of energy resources (thermal, wind, and solar). The output power from wind or solar generator has two probabilities either underestimation or overestimation consequently. These two probabilities have been translated into the objective function by two extra costs, penalty cost, and reserve cost, respectively. To check the validity of the proposed algorithm, it is applied to a modified IEEE-30 and IEEE-57 bus systems. The obtained results are compared with some recent optimization methods. The results show the effectiveness of marine predator algorithm in providing the optimal solution for the power flow problem with maintaining the power system constraints inviolate.

1. Introduction

OPF has verified its validity for providing the secure and efficient operation of various power systems since 1962, the date of its inception [1]. OPF has the main goal represents in finding the optimal settings related to the control variables of the power system with definite objective functions taking into consideration maintaining the system constraints within the predefined limits. The control variables of the power system consist of active power, generator buses voltage, and transformer tap settings. The system constraints have to be maintained, such as the capacity of transmission lines, the balance of power flow, the voltage of all system buses, and the capability of power generators. Many conventional optimization algorithms have been utilized for solving the OPF problem. These algorithms are classified as mixed-integer linear programming, quadratic programming, interior-point algorithms, and nonlinear programming [2]. However, these conventional algorithms need to linearize the objective function first. Thus, they are suitable only for nondifferentiable, nonconvex, and non-smooth objective functions. To avoid this problem, many metaheuristic optimization algorithms have been provided to solve the OPF problem that will be discussed later in the related work section. In this paper, a recent metaheuristic optimization algorithm, the marine predator algorithm (MPA), is applied for solving the OPF problem considering the uncertainty of wind and solar PV production. The MPA is chosen for this study due to its effectiveness in solving complicated problems in many different fields [3,4]. The main work of this paper is as follows:

(i) Modifying the IEEE- 30 bus system to include two types of renewable energy generators by replacing the two TPGs connected at bus 5 and bus 11 with two wind power generators (WPGs) and replacing the TPG connected at bus 13 with solar photovoltaic generator (SPG).

(ii) Forming the stochastic models of the WPGs and the SPG.

(iii) Applying the proposed MPA to solve the OPF problem for the modified IEEE-30 bus power system.

(iv) Analyzing the results obtained by MPA with the results obtained by other three recent optimization algorithm, particle swarm optimization (PSO) [5], modified particle swarm optimization (MPSO) [6], and genetic algorithm (GA) [7], in addition to the results of SHADE-SF algorithm provided in [8] to verify its validity for solving the OPF problem.

(v) Studying the impact of varying the penalty and reserve cost coefficients of WPGs and SPGs on the optimal scheduled powers and their costs of production.

(vi) Modifying the IEEE-57 bus system by replacing the two TPGs connected at bus 2 and bus 6 with two wind power generators (WPGs) and replacing the TPG connected at bus 9 with solar photovoltaic generator (SPG).

(vii) Applying the proposed MPA to solve the OPF problem for the modified IEEE-57 bus power system, and analyzing the results obtained by MPA with the results of GA.

The other parts of this paper are ordered as follows: Section 2 presents the related work. Then, Section 3 illustrates the formulation of the OPF problem. Section 4 shows the stochastic models of both WPGs and SPG. Then, Section 5 presents the proposed optimization algorithm. The simulation results are provided in Section 6. Finally, Section 7 provides the conclusions of this study.

2. Related Work

In recent literature, traditional OPF that deals with thermal power generators (TPGs) has been extensively studied. In [9], the authors have presented a method for solving the alternating current optimal power flow (ACOPF) problem based on combination between various tuning methods and a sequential linear programming approach. The authors in [10] have proposed an effective whale optimization algorithm for solving optimal power flow problems (EWOA-OPF) with application on four different standard IEEE bus test systems to optimize single- and multiobjective functions under the system constraints. In [11], a novel fuzzy adaptive hybrid configuration oriented to a joint self-adaptive particle swarm optimization (SPSO) and differential evolution algorithms (FAHSPSO-DE) has been proposed to address the multiobjective OPF (MOOPF) problem. In [12], a modified grasshopper optimization algorithm (MGOA) is proposed to solve the optimal power flow (OPF) problem. An improved gray wolf optimization algorithm (I-GWO) based on the dimension learning-based hunting (DLH) search strategy has been presented in [13] for solving the OPF problem. However, the OPF problem considering both TPGs and RESs became an attractive topic for many researchers due to the challenges caused by RESs in the planning and operation of power systems. In [14], the authors developed a new golden ratio optimization method (GROM) algorithm to provide a solution for the OPF problem in a power system including wind and solar units. In [15], a gray wolf optimization algorithm (GWO) is applied to reach the optimal solution of power flow problem including wind and solar photovoltaic resources in a modified IEEE-30 bus and IEEE-57 bus power systems.

A new Manta Ray Foraging Optimization (MRFO) algorithm is developed in [16] to solve the OPF with and without renewable energy resources. The authors in [17] have applied the flower pollination algorithm (FPA) to solve an OPF problem IEEE-30 bus power system modified by solar photovoltaic, wind, and small hydro power units. In [18], the authors have proposed a particle swarm optimization (PSO) algorithm to solve the OPF for a power system including renewable energy resources and storage systems. The authors in [8] have proposed a combination between the success history based adaptive differential evolution (SHADE) technique and the superiority of feasible solutions (SF) technique to develop an efficient algorithm called SHADE-SF for solving the OPF incorporating wind and solar resources.

3. Problem Formulation

In this section, the cost models of all three types of power generators used in the modified power system are presented as follows.

3.1. Cost Model for TPGs. The total generation cost of TPGs in ($/h) considering the valve point effect is calculated as follows:

$$C_{T0}\left(P_{\mathrm{TG}}\right) = \sum_{i=1}^{N_{TG}} a_i + b_i P_{\mathrm{TG}i} + c_i P_{\mathrm{TG}i}^2 + \left| l_i * \ \sin\left(m_i * \left(P_{\mathrm{TG}i}^{\min} - P_{\mathrm{TG}i}\right)\right)\right|, \tag{1}$$

where $P_{\mathrm{TG},i}$ is the output power of the i-th TPG and its cost coefficients are represented by a_i, b_i, and c_i. N_{TG} refers to the number of TPGs in the power systems l_i and m_i are valve-point loading coefficients. $P_{\mathrm{TG}i}^{\min}$ indicates the minimum power of i-th TPG.

All cost coefficients of TPGs needed for calculations have been mentioned in Tables 1 and 2.

3.2. Direct Generation Cost of SPG and WPGs. The direct generation cost of $WPG_{,j}$ in relevant to its scheduled output power is calculated by (2)as follows:

$$C_{wdr\ ,j} = d_j P_{wdsch,j}, \tag{2}$$

where $P_{wds\ ch,j}$ represents the output power scheduled from WPG and j and d_j are its direct cost coefficient.

Likewise, the direct generation cost of SPG,k is calculated by the following:

$$C_{s\ dr\ ,k} = e_k P_{slch,k}, \tag{3}$$

where e_k represents the coefficient of direct cost associated with $SPG_{,k}$, while $P_{slsch,k}$ denotes the output power scheduled from the $SPG_{,k}$.

3.3. Cost Assessment of Uncertain Output of WPG. There are two situations that may happen due to the intermittent nature of wind power. The first one takes place when the actual output power of WPG is lower than the anticipated output. This situation is referred to as overestimation, thus committing the spinning reserve will be necessary to overcome this situation and as a result, requires a reserve cost which is calculated as follows:

$$C_{wdr,j}\left(P_{wdsch,j} - P_{wdav,j}\right) = K_{rwd,j}\left(P_{wdsch,j} - P_{wdav,j}\right) = K_{rwd,j}\int_0^{P_{wdsch,j}} \left(P_{wdsch,j} - P_{wd,j}\right) f_{wd}\left(P_{wd,j}\right) \mathrm{d}P_{wd,j}, \tag{4}$$

where $P_{wda\ v,j}$ denotes the available power of $WPG_{,j}$ and $K_{RW,j}$ refers to its coefficient of reserve cost, while $f_{wd}(P_{wd,j})$ represents the Weibull PDF of $WPG_{,j}$ output power.

In contrast, the second situation, which refers to underestimation, will happen when the power output from WPG is greater than the expected value, a penalty cost corresponding to the remaining wind power should be compensated by the system operator as illustrated in (5).

$$C_{wdp\ ,j}\left(P_{wdav,j} - P_{wdsch,j}\right) = K_{Pwd,j}\left(P_{wdav,j} - P_{wdsch,j}\right) = K_{Pwd,j}\int_{P_{Wds\ ch,j}}^{P_{Wdr\ ,j}} \left(P_{wd,j} - P_{wdsch,j}\right) f_{wd}\left(P_{wd,j}\right) \mathrm{d}P_{wd,j}, \tag{5}$$

where $K_{pwd,j}$ denotes the coefficient of penalty cost. $P_{wd,j}$ refers to the rated output power related to the $WPG_{,j}$.

3.4. Cost Assessment of Uncertain Output of SPG. The output power of SPG is also intermittent which may arise the overestimation and underestimation situations similar to wind power. In overestimation situation, the reserve cost of $SPG_{,k}$ is represented by the following:

$$C_{slr,k}\left(P_{slsch,k} - P_{sav,k}\right) = K_{rs,k}\left(P_{ssch,k} - P_{sav,k}\right) = K_{rsl,k} * f_{sl}\left(P_{slav,k} < P_{slsch,k}\right) * \left[\left(P_{slsch,k} - E\left(P_{slav,k} < P_{slsch,k}\right)\right]\right], \tag{6}$$

where $K_{rsl,k}$ refers to the coefficient of reserve cost for $SPG_{,k}$, $P_{slav,k}$ refers to the available output power from the same SPG, and $f_{sl}(P_{slav,k} < P_{slsch,k})$ denotes the shortage occurrence probability in the solar power production, and $E(P_{slav,k} < P_{slsch,k})$ denotes the expectation of being the output of SPG below the $P_{slsch,k}$.

While, in underestimation situation, the penalty cost of $SPG_{,k}$ is calculated as follows:

Table 1: Cost coefficients of TPGs for the IEEE-30 bus system [19].

TPG #	Bus	a	b	c	l	m
1	1	0	2	0.00375	18	0.037
2	2	0	1.75	0.0175	16	0.038
3	8	0	3.25	0.00834	12	0.045

Table 2: Cost coefficients of TPGs for the IEEE-57 bus system [19, 20].

TPG #	Bus	a	b	c	l	m
1	1	0	20	0.0775795	18	0.037
2	3	0	20	0.25	13.5	0.041
3	8	0	20	0.0222222	14	0.04
4	12	0	20	0.0322581	12	0.045

$$C_{slp,k}\left(P_{slav,k}-P_{slsch,k}\right)=K_{psl,k}\left(P_{slav,k}-P_{slsch,k}\right)=K_{psl,k}*f_{sl}\left(P_{slav,k}>P_{slsch,k}\right)*\left[\left(E\left(P_{slav,k}<P_{slsch,k}\right)-P_{slsch,k}\right],\quad(7)$$

where $K_{psl,k}$ indicates the coefficient of penalty cost, $f_{sl}(P_{slav,k}>P_{slsch,k})$ is the outstanding probability of solar output power from the $SPG_{,k}$ comparing to $P_{slsch,k}$, while $E(P_{slav,k}<P_{slsch,k})$ refers to the anticipated outstanding output from the $SPG_{,k}$.

3.5. Objective Function. The objective function (F) of the OPF is formulated to minimize the total generation cost including the cost models presented from (1) to (7).

$$\begin{aligned}F=&C_T\left(P_{\mathrm{TG}}\right)+\sum_{j=1}^{N_{\mathrm{WG}}}\left[d_jP_{wdsch,j}+K_{rwd,j}\left(P_{wdsch,j}-P_{wdav,j}\right)+K_{Pwd,j}\left(P_{wdav,j}-P_{wdsch,j}\right)\right]\\&+\sum_{j=1}^{N_{\mathrm{SG}}}\left[e_kP_{slsch,k}+K_{Rsl,k}\left(P_{slsch,k}-P_{slav,k}\right)+K_{psl,k}\left(P_{slav,k}-P_{slsch,k}\right)\right],\end{aligned}\quad(8)$$

where N_{SG} and N_{WG} are the number of SPGs and WPGs, respectively.

3.5.1. Equality Constraints. Equality constraints of the power system are represented as follows [8]:

$$P_{Gi}=P_{Di}+V_i\sum_{i=1}^{\mathrm{NB}}V_j\left[G_{ij}\cos\left(\delta_{ij}\right)+B_{ij}\sin\left(\delta_{ij}\right)\right],\quad i\in\mathrm{NB},\quad(9)$$

$$Q_{Gi}=Q_{Di}+V_i\sum_{i=1}^{NB}V_j\left[G_{ij}\sin\left(\delta_{ij}\right)-B_{ij}\cos\left(\delta_{ij}\right)\right],\quad i\in\mathrm{NB}.\quad(10)$$

3.5.2. Inequality Constraints. Inequality constraints of the power system are represented as follows:

(i) Generator constraints (renewable or thermal as applicable):

$$P_{Gi}^{\min}\le P_{Gi}\le P_{Gi}^{\max},\quad i=1,\ldots,N_G,\quad(11)$$

$$Q_{Gi}^{\min}\le Q_{Gi}\le Q_{Gi}^{\max},\quad i=1,\ldots,N_G,\quad(12)$$

$$V_{Gi}^{\min}\le V_{Gi}\le V_{Gi}^{\max},\quad i=1,\ldots,N_G.\quad(13)$$

(ii) Security constraints:

Equation (14) denotes the voltage limits subjected to load buses, while (15) provides the capacity constraints of transmission lines, where NL denotes the number of transmission lines in the power system.

$$V_{L_p}^{\min}\le V_{L_p}\le V_{L_p}^{\max},\quad p=1,\ldots,N_L,\quad(14)$$

$$S_{L_q}\le S_{L_q}^{\max},\quad q=1,\ldots,N_L.\quad(15)$$

3.5.3. Power Losses (P_{loss}). P_{loss} is determined by the following:

$$P_{\mathrm{loss}}=\sum_{i=1}^{\mathrm{NL}}\sum_{j\neq1}^{\mathrm{NL}}G_{ij}V_i^2+V_j^2-2V_iV_j\cos\left(\delta_{ij}\right),\quad(16)$$

δ_{ij} stands for the voltage angles difference between bus i and bus j, while, G_{ij} is the transfer conductance.

3.5.4. Voltage Deviation. Voltage deviation indicates the cumulative load buses voltage deviation from 1.0 (p.u.) as follows:

$$V_d=\sum_{p=1}^{\mathrm{NL}}\left|V_{Lp}-1\right|.\quad(17)$$

4. Stochastic Modeling of RESs

The distribution of wind speed is suitable with Weibull probability density function (PDF) [21, 22]. The wind speed probability (W_v) following Weibull PDF is determined as follows:

$$f_{W_v}(W_v)=\left(\frac{k}{c}\right)+\left(\frac{W_v}{c}\right)^{(k-1)}e^{-\left(W_v/c\right)^{ck}},\quad\text{for } 0<W_v<\infty,\quad(18)$$

where k and c stand for shape factor and scale factor, respectively. The mean of Weibull distribution is determined as follows:

$$M_{wbl}=c*\Gamma\left(1+k^{-1}\right).\quad(19)$$

In (19), the symbol Γ represents gamma function which is given by the following:

$$\Gamma(x)=\int_0^{\infty}e^{-t}t^{x-1}\mathrm{d}t.\quad(20)$$

Figures 1 and 2 provide the wind frequency distribution depending on Weibull fitting after running 8000 Monte-Carlo simulation scenarios [8].

The output power of SPG affects by the solar irradiance (I) based on lognormal PDF [23]. This concept is illustrated in (21):

$$f_I(I) = \frac{1}{I\sigma\sqrt{2\pi}} \exp\left\{\frac{-(\ln\ x - \mu)^2}{2\sigma^2}\right\}, \quad \text{for } I > 0, \tag{21}$$

where $f_I(I)$ denotes the irradiance probability, μ denotes the mean and of lognormal PDF and σ represents the standard deviation.

$$M_{\text{lgn}} = \exp\left(\mu + \frac{\sigma^2}{2}\right). \tag{22}$$

Figure 3 provides the lognormal PDF for the SPG after running 8000 Monte-Carlo scenarios.

The chosen values of Weibull and lognormal PDFs are mentioned in Tables 3 and 4.

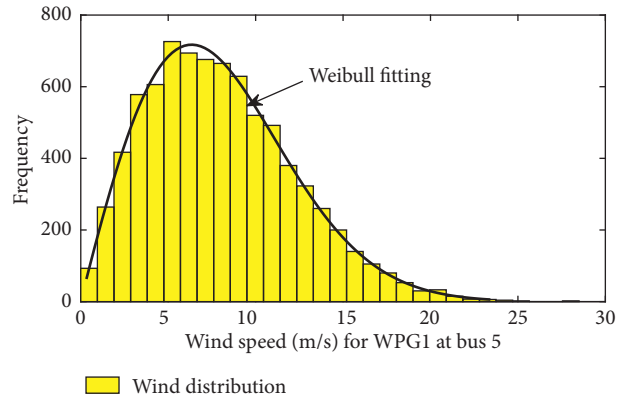

Figure 1: Wind speed distribution for WPG1.

4.1. Modeling of WPGs. The power output from WPG affects the speed of wind. The formula of power output from wind turbine is provided in [8] as follows:

$$P_{wd}(W_v) = \begin{cases} 0, & \text{for } W_v < W_{vin} \text{ and } W_v > W_{vout}, \\ P_{wdr}\left(\dfrac{(W_v - W_{vin})}{(W_{vr} - W_{vin})}\right), & \text{for } W_{vin} \le W_v \le W_{vr} \text{ (continous zone)}, \\ P_{wdr}, & \text{for } W_{vr} \le W_v \le W_{vout} \text{ (discrete zone)}, \end{cases} \tag{23}$$

where W_{vin} denotes the cut-in speed, W_{vout} represents the cut-out speed, and W_{vr} stands for the rated wind speed. P_{wdr} indicates the rated power of the wind turbine.

The probabilities of power output from WPG in the discrete zone can be determined by [24]:

$$\begin{aligned} f_{wd}(P_{wd})\{P_{wd} = 0\} &= 1 - \exp\left[-\left(\frac{W_{vin}}{c}\right)^k\right] + \exp\left[-\left(\frac{W_{vout}}{c}\right)^k\right], \\ f_{wd}(P_{wd})\{P_{wd} = P_{wdr}\} &= \exp\left[-\left(\frac{W_{vr}}{c}\right)^k\right] - \exp\left[-\left(\frac{W_{vout}}{c}\right)^k\right]. \end{aligned} \tag{24}$$

While in the continuous zone, the probabilities of power output from WPG are determined by [24]:

$$f_{wd}(P_{wd}) = \frac{k(W_{vr} - W_{vin})}{c^k * P_{wdr}}\left[W_{vin} + \frac{P_{wd}}{P_{wdr}}(W_{vr} - W_{vin})\right]^{k-1} * \exp\left[-\left(\frac{W_{vin} + (P_w/P_{wr})(W_{vr} - W_{vin})}{c}\right)^k\right]. \tag{25}$$

4.2. Modeling of SPG. In the same way, the solar irradiance versus the energy conversion of the SPG is provided in [25] as follows:

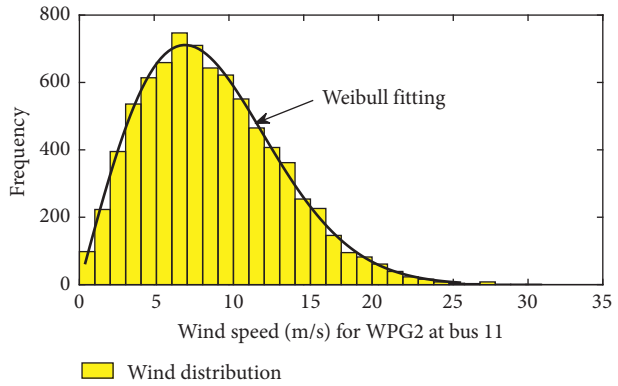

Figure 2: Distribution of wind speed for WPG2.

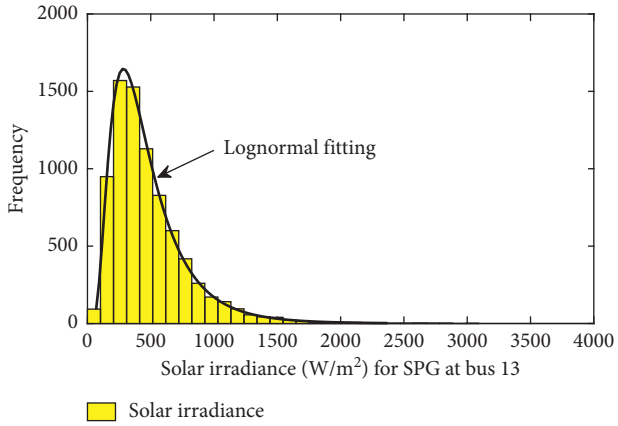

Figure 3: Solar irradiance distribution for SPG.

Table 3: Weibull and lognormal PDF parameters for WPGs and SPG for the IEEE-30 bus system.

	WPGs				SPG		
WPG#	No. of turbines	Rated power P_{wr}	Weibull PDF parameters	Weibull mean, M_{wbl}	Rated power, P_{sr}	Lognormal PDF parameters	Lognormal mean, M_{logn}
1 (at bus 5)	25	75 MW	$k=2,\ c=9$	$v=7.976$ (m/s)	50 MW (at bus 13)	$\delta=0.6,\ \mu=6$	I = 483 (W/m^2)
2 (at bus 11)	20	60 MW	$k=2,\ c=10$	$v=8.862$ (m/s)			

Table 4: Weibull and lognormal PDF parameters for WPGs and SPG for the IEEE-57 bus system.

	WPGs				SPG		
WPG#	No. of turbines	Rated power P_{wr}	Weibull PDF parameters	Weibull mean, M_{wbl}	Rated power, P_{sr}	Lognormal PDF parameters	Lognormal mean, M_{logn}
1 (at bus 2)	25	100 MW	$k=2,\ c=9$	$v=7.976$ (m/s)	100 MW (at bus 9)	$\delta=0.6,\ \mu=6$	I = 483 (W/m^2)
2 (at bus 6)	25	100 MW	$k=2,\ c=10$	$v=8.862$ (m/s)			

$$P_{sl}(I) = \begin{cases} P_{slr}\left(\dfrac{I^2}{I_{st\,d} R_c}\right), & \text{for } 0 < I < R_c, \\ P_{slr}\left(\dfrac{I}{I_{st\,d}}\right), & \text{for } I \geq R_c, \end{cases} \tag{26}$$

where $I_{st\,d}$ denotes the solar irradiance in a standard environment (800 W/m^2), R_c indicates a specific irradiance amount (120 W/m^2), and P_{slr} denotes the rated actual power of SPG.

The overestimation and underestimation costs of the power produced from the SPG are calculated by (27) and (28) respectively.

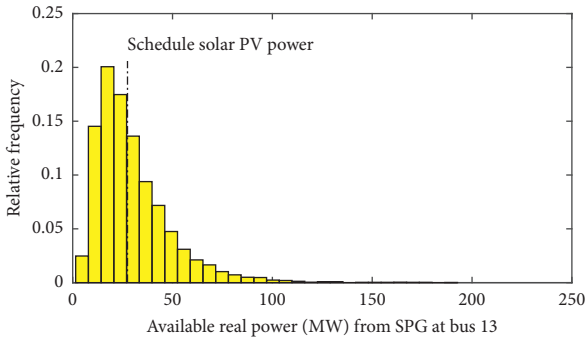

Figure 4: Actual power distribution for the SPG.

$$C_{slr,k}(P_{slsch} - P_{slav}) = K_{rsl}(P_{slsch} - P_{slav}) = K_{rsl} \sum_{n=1}^{N^-} [P_{slsch} - P_{s\,\ln-}] * f_{s\,\ln-}, \tag{27}$$

$$C_{slp,k}(P_{slav} - P_{slsch}) = K_{psl}(P_{slav} - P_{slsch}) = K_{psl} \sum_{n=1}^{N^+} [P_{s\,\ln+} - P_{slsch}] * f_{s\,\ln+}, \tag{28}$$

where P_{sln+} and P_{sln-} denote the surplus and shortage powers represented by the left and right half planes of the schedule power of SPG (P_{slsch}) provided in Figure 4. f_{sln+} and f_{sln-} stand for the relative frequencies of the $P_{s\,\ln+}$ and $P_{s\,\ln-}$ occurrence. N^+ and N^- denote the number of discrete bins on the right and left planes of schedule power of SPG.

5. Optimization Algorithm

The marine predator algorithm (MPA) has been developed by Faramarzi et al. [26]. The MPA simulates the strategy of optimal searching of the marine predators (MPs) during detecting their prey as follows: MPs prefer to follow the Lévy behavior when the concentration of prey is low, while they follow the Brownian behavior when there is abundant prey [27, 28].

The process of MPA has three main phases based on the velocity ratio as follows:

5.1. Phase 1. This phase happens when the velocity ratio is high and it is expressed as follows:

while Iter < (1/3)Max_Iter

$$\begin{aligned} \overrightarrow{\text{stepsize}_i} &= \overrightarrow{R_B} \otimes \left(\overrightarrow{\text{Elite}_i} - \overrightarrow{R_B} \otimes \overrightarrow{\text{Prey}_i}\right), \quad i = 1, \ldots, n, \\ \overrightarrow{\text{Prey}_i} &= \overrightarrow{\text{Prey}_i} + \text{P}.\overrightarrow{R} \otimes \overrightarrow{\text{stepsize}_i}, \end{aligned} \tag{29}$$

where Iter represents the present iteration and Max_Iter refers to the maximum iterations number, while $\overrightarrow{R_B}$ refers to a vector contains random numbers depending on Brownian distribution. The sign $\otimes$ is needed for providing the entry wise multiplications. The constant P equals 0.5 and $\overrightarrow{R}$ has a range from 0 to 1.

5.2. Phase 2. This phase takes place when the velocity ratio is unity. Step by step, the exploration changes to exploitation as follows:

While, (1/3)Max_Iter < Iter < (2/3)Max_Iter

In the 1st half of the population:

$$\begin{aligned} \overrightarrow{\text{stepsize}_i} &= \overrightarrow{R_L} \otimes \left(\overrightarrow{\text{Elite}_i} - \overrightarrow{R_L} \otimes \overrightarrow{\text{Prey}_i}\right), \quad i = 1, \ldots, \frac{n}{2}, \\ \overrightarrow{\text{Prey}_i} &= \overrightarrow{\text{Prey}_i} + P.\overrightarrow{R} \otimes \overrightarrow{\text{stepsize}_i}, \end{aligned} \tag{30}$$

where $\overrightarrow{R_L}$ denotes a random numbers vector depending on Lévy distribution. $\overrightarrow{R_L} \otimes \overrightarrow{\text{Prey}_i}$ simulates the prey movement in Lévy manner, while adding the $\overrightarrow{\text{stepsize}_i}$ to prey position acts out the prey movement.

In the 2nd half of the population,

$$\begin{aligned} \overrightarrow{\text{stepsize}_i} &= \overrightarrow{R_B} \otimes \left(\overrightarrow{R_B} \otimes \overrightarrow{\text{Elite}_i} - \overrightarrow{\text{Prey}_i}\right), \quad i = \frac{n}{2}, \ldots, n, \\ \overrightarrow{\text{Prey}_i} &= \overrightarrow{\text{Elite}_i} + P.\text{CF} \otimes \overrightarrow{\text{stepsize}_i}, \end{aligned} \tag{31}$$

where CF = $(1 - (\text{Iter}/\text{Max\_Iter}))^{(2(\text{Iter}/\text{Max\_Iter}))}$

CF refers to an adaptive parameter considered to control the $\overrightarrow{\text{stepsize}_i}$ for the movement of the predator. $\overrightarrow{R_B} \otimes \overrightarrow{\text{Elite}_i}$ simulates the predator movement in Brownian behavior, while the position of prey is updated depending on the predator movement in Brownian behavior.

5.3. Phase 3. This phase happens when the velocity ratio is low as follows:

While Iter > (2/3)Max_Iter,

$$\begin{aligned}\overrightarrow{\text{stepsize}_i} &= \overrightarrow{R_L} \otimes \left(\overrightarrow{R_L} \otimes \overrightarrow{\text{Elite}_i} - \overrightarrow{\text{Prey}_i}\right), \quad i = 1, \ldots, n,\\ \overrightarrow{\text{Prey}_i} &= \overrightarrow{\text{Elite}_i} + P.\text{CF} \otimes \overrightarrow{\text{stepsize}_i}.\end{aligned} \tag{32}$$

5.4. Eddy Formation and FADs' Effect. Another important point that may cause a change in MPs behavior is the environmental issues like the fish aggregating devices (FADs) effects and the eddy formation. The FADs can be considered as a local optima and their effects are mathematically formed as follows:

$$\overrightarrow{\text{Prey}_i} = \begin{cases} \overrightarrow{\text{Prey}_i} + \text{CF}\left[\overrightarrow{X_{\min}} + \overrightarrow{R} \otimes \left(\overrightarrow{X_{\max}} - \overrightarrow{X_{\min}}\right)\right] \otimes \overrightarrow{U}, & \text{if } r \le \text{FADs}, \\ \overrightarrow{\text{Prey}_i}\,[\text{FADs}\,(1-r) + r]\left(\overrightarrow{\text{Prey}_{r1}} - \overrightarrow{\text{Prey}_{r2}}\right), & \text{if } r > \text{FADs}, \end{cases} \tag{33}$$

where FADs = 0.2 represents the probability of FADs effects on the whole optimization process. $\overrightarrow{U}$ refers to the vector of binary with arrays including 0 and 1. This random vector changes its array to 0 if the array is lower than 0.2, and changes its array to 1 if it is larger than 0.2. r represents the uniform random number in [0, 1]. $\overrightarrow{X_{\max}}$ and $\overrightarrow{X_{\min}}$ represent the vector that contains the upper and lower bounds of dimensions. r_1 and r_2 are random indexes of the prey matrix. Figure 5 shows the pseudocode of the MPA.

6. Results and Discussion

In this section, five case studies are implemented as follows.

(i) Case1 is performed to check the ability of the MPA to achieve the minimum cost of power generation in the modified IEEE-30 bus system.

(ii) Case 2 is applied to study the impact of varying the penalty cost coefficients of WPGs and SPG on their scheduled output powers and the corresponding costs.

(iii) Case 3 is performed to study the impact of varying the reserve cost coefficients of WPGs and SPG on their scheduled output powers and the corresponding costs.

(iv) Case 4 is implemented to study the effect of the variation in scale parameter (c) of the Weibull PDF and lognormal PDF mean parameter (μ) on the different costs of wind power and solar power respectively.

(v) Case 5 is implemented to check the ability of the MPA to achieve the minimum cost of power generation in the modified IEEE-57 bus system.

The simulation process is performed by MATLAB software and computer properties as follows:

(i) Processor: Intel (R) Core (TM) i3 CPU M380 @2.53 GHz,

(ii) Installed memory (RAM): 4 GB.

The algorithms have been run for 10 times with a maximum of 500 iterations for each run as the criteria of ending the run.

6.1. Case 1: Minimization of Total Generation Cost for the Modified IEEE-30 Bus Power System. This case study is applied to minimize the total cost of generation using the MPA based on equation (8) with maintaining the constraints of the system inside their predefined limits. The detailed parameters of the modified IEEE-30 bus power system used in this case are stated in Table 5.

The direct cost coefficients of the WPGs are $d_1 = 1.6$ and $d_2 = 1.75$. Penalty cost coefficient for not fully utilized wind power is assumed as $K_{\text{pwd},1} = K_{\text{pwd},2} = 1.5$ and reserve cost coefficient for overestimation is $K_{\text{rwd},1} = K_{\text{rwd},2} = 3$.

The direct, penalty, and reserve cost coefficients for SPG are proposed to be $e = 1.6$, $K_{\text{psl}} = 1.5$, and $K_{\text{rsl}} = 3$, respectively.

Table 6 provides the optimal results obtained by MPA through all runs. It also provides the results of other implemented algorithms, MPSO, PSO, and GA, in addition to the results of SHADE-SF provided in Ref. [8] to check the results of MPA with other optimization algorithms. The statistical details values of total generation cost with maximum, minimum, mean, and standard deviation over 10 runs of each algorithm are recorded in Table 7. The simulation results indicate the effectiveness of MPA in terms of total cost minimization as it achieved the minimum total cost, 781.924 ($/h) compared to other algorithms which have a fast convergence compared to MPA, but they lied on the local optima problem.as shown in Figure 6.

The profile voltage of generator buses is within the lower and upper limits for the IEEE-30 bus system as recorded in Table 6 and illustrated in Figure 7.

The generator reactive power is dependent or state variable in the OPF problem. The reactive power constraints should be satisfied after the optimization process. The generator reactive powers obtained through the MPA are within the predefined limits as observed from Table 6. The constraints forced on the load buses voltages are also critical issue in the OPF problem. In this work, the voltages of all load buses are within their limits as shown in Figure 8.

6.2. Case 2: Studying the Impact of Varying the Penalty Cost Coefficients of WPGs and SPG. For this case, reserve cost coefficients of WPGs and SPG are kept constant at its initial value (KR = 3) in case1, while the penalty cost coefficients are increased from its initial value (KP = 1.5) in case1 to 3 in case

```
Initialize Prey populations i=1,...,n
While finish criteria is not met
 Calculate the fitness and construct the Elite matrix
  If Iter < Max_Iter/3
    Update prey based on (30)
  Else if Max_Iter/3<Iter<2*Max_Iter/3
    For the first half of the populations (i=1,...,n/2)
    Update prey based on (31)
    For the other half of the populations (i=n/2,...,n)
    Update prey based on (32)
  Else if Iter >2*Max_Iter/3
    Update prey based on (33)
  End (if)
   Accomplish memory saving and Elite update
   Applying FADs effect and update based on (34)
End While
```

Figure 5: Pseudocode of the MPA.

Table 5: Summary of the modified IEEE-30 bus power system [8].

Item	Number	Details
Buses	30	[29]
Branches	41	[29]
TPGs	3	Linked at bus 1 (swing), bus 2 and bus 8
WPGs	2	Linked at bus 5 and bus11
SPG	1	Linked at bus 13
Control variables	11	The scheduled power output from: TPG2, TPG3, WPG1, WPG2, SPG, and generator buses voltages (6 generators)
System load	—	283.4 MW, 126.2 MVAr
Permissible load buses voltage range	24	[0.95–1.05] p.u.

Table 6: OPF simulation results-case 1.

	Min	Max	MPA	MPSO	PSO	GA	SHADE-SF [8]
Control variables							
P_{TG1} (MW)	50	140	134.9079	134.9079	134.9224	134.8295	134.908
P_{TG2} (MW)	20	80	26.5717	27.38553	27.93474	27.0371	28.564
P_{TG3} (MW)	10	35	10	10	10	10	10
$P_{wdsch,1}$ (MW)	0	75	42.7653	43.21138	42.80075	45.9888	43.774
$P_{wdsch,2}$ (MW)	0	60	36.0224	36.67773	37.00976	34.7516	36.949
P_{slsch} (MW)	0	50	38.9318	37.11847	36.65468	36.5856	34.976
V_1 (p.u.)	0.95	1.1	1.07228	1.069438	1.068328	1.0737	1.072
V_2 (p.u.)	0.95	1.1	1.0571	0.95	0.952723	1.0559	1.057
V_5 (p.u.)	0.95	1.1	1.0349	1.1	1.155915	1.0634	1.035
V_8 (p.u.)	0.95	1.1	1.0396	1.1	1.098617	1.041	1.04
V_{11} (p.u.)	0.95	1.1	1.0989	1.1	1.700761	1.0725	1.1
V_{13} (p.u.)	0.95	1.1	1.0531	1.1	1.215303	1.041	1.055
Parameters							
Q_{TG1} (MVAr)	−20	150	−1.5712	8.4244	7.744306	4.7857	−1.903
Q_{TG2} (MVAr)	−20	60	13.3449	−20	−20	0.7989	13.261
Q_{TG3} (MVAr)	−15	40	35.056	40	40	39.97941	35.101
$Q_{wdsch,1}$ (MVAr)	−30	35	23.3788	35	35	35	23.181
$Q_{wdsch,2}$ (MVAr)	−25	30	30	29.0507	30	21.79221	30
Q_{slsch} (MVAr)	−20	25	16.8558	25	25	13.85258	17.346
Total generation cost ($/h)			**781.924**	782.9268	782.3851	782.8023	782.503
P_{loss} (MW)			5.78	5.9	5.92	5.793	5.77
V_d (p.u.)			0.4587	0.551	0.5487	0.44393	0.463

Table 7: Statistical details values of total generation cost ($/h) -case 1.

Algorithm	Max.	Min.	Mean	Std. dev.
MPA	782.6771	**781.924**	782.3531	**0.2474**
MPSO	786.06	782.9268	783.9104	0.9685
PSO	783.2811	782.3851	782.7661	0.2601
GA	784.2214	782.8023	783.1872	0.3809

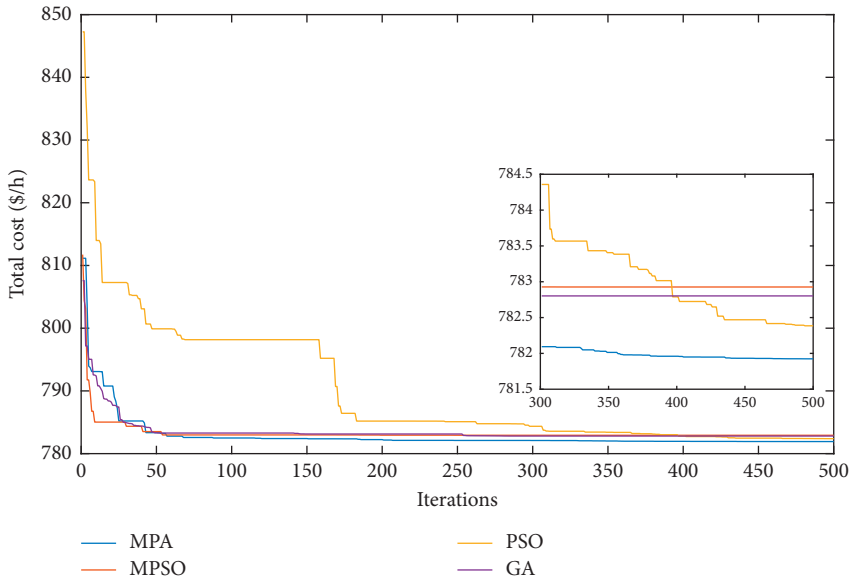

Figure 6: Convergence characteristics-case 1.

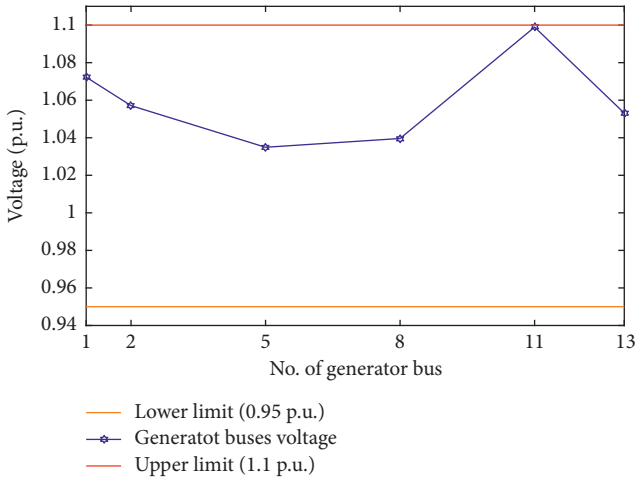

Figure 7: Profile voltage of generator buses–case1.

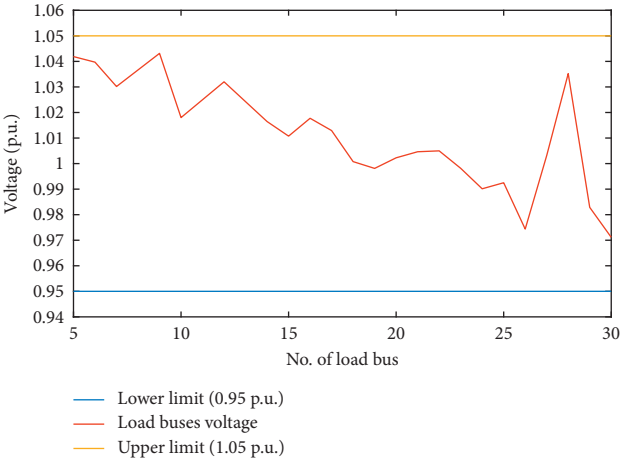

Figure 8: Voltages profile of load buses-case 1.

2a and 4 in case 2b to study the impact of this increasing on the scheduled powers of the existence power generators in the modified power system and their corresponding costs.

Figure 9 shows the impact of varying the penalty cost coefficients on the power scheduled from all generators in the modified system. It is expected with increasing the penalty cost coefficients, the powers scheduled from WPGs and SPG increases because this will help in decreasing the penalty cost. This is observed from Figure 9 as the scheduled power of WPGs increases with increasing the penalty cost coefficient. However, this did not occur with the scheduled power of SPG, as a fluctuation in its scheduled power is observed. This fluctuation can be interpreted by its stochastic nature.

Consequently, with increasing the value of penalty cost coefficients, a slight decrease in thermal power cost occurs, while the cost of solar power increases slightly and the cost of wind power increases significantly leading to an observed increase in the total generation cost as shown in Figure 10.

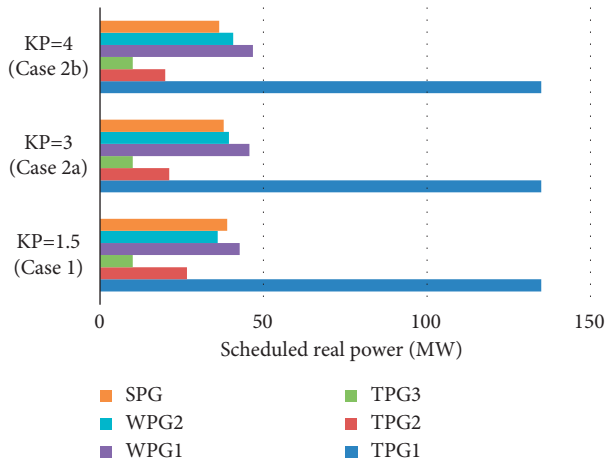

Figure 9: Scheduled active powers (MW) vs. penalty cost coefficients.

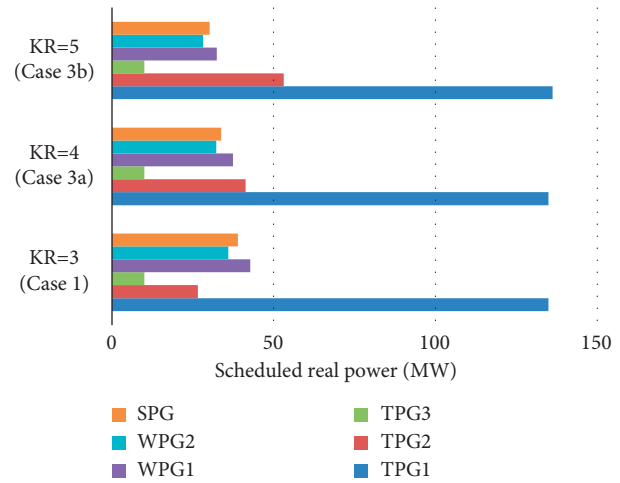

Figure 11: Scheduled active powers (MW) vs. reserve cost coefficients.

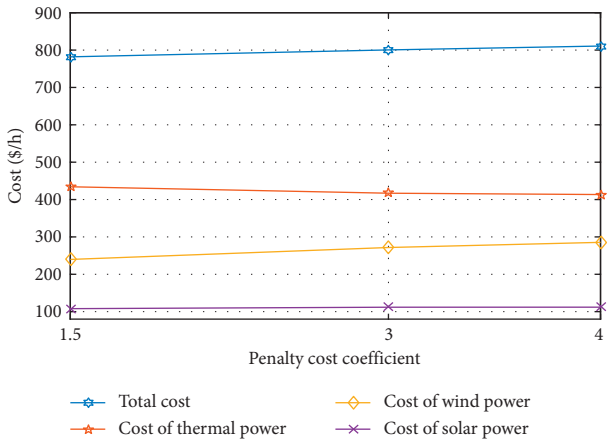

Figure 10: Curves of different costs with changing penalty cost coefficients.

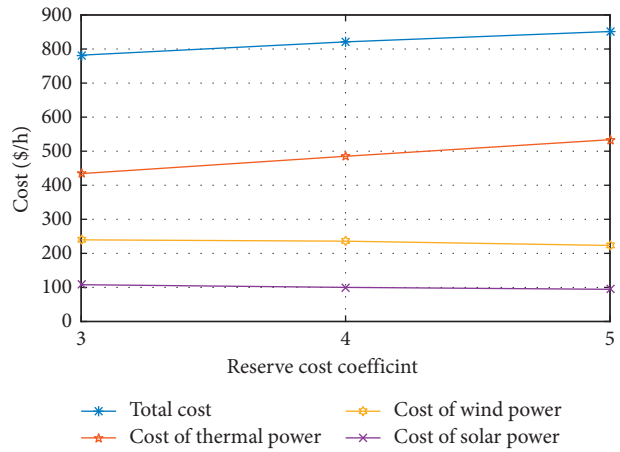

Figure 12: Curves of different costs with changing reserve cost coefficients.

6.3. Case 3: Studying the Impact of Varying the Reserve Cost Coefficients of WPGs and SPG. In this case, the penalty cost coefficients of WPGs and SPG are kept constant at its initial value (KP = 1.5) in case of 1, while the reserve cost coefficients are increased from its initial value (KR = 3) in cases 1 to 4 in case 3a and 5 in case 3b to study the impact of this increasing on the scheduled powers of the existence power generators in the modified power system and their corresponding costs.

Similar to Case 2, Figure 11 presents the impact of changing the reserve cost coefficients on the scheduled power of all generators. It is noticed that with increasing the values of reserve cost coefficients of WPGs and SPG, the scheduled power from WPGs and SPG decreases as expected because reducing them requires a lower spinning reserve level.

As a result, with increasing the reserve cost coefficients, the cost of scheduled power from WPGs and SPG decreases as observed from Figure 12, while the cost of scheduled power from TPGs increases significantly leading to a high increase in the total generation cost because the TPGs are used as a compensation to the shortage in the scheduled power from WPGs and SPG.

6.4. Case 4: Different Costs against the PDF Parameter of WPGs and SPG. This case study is performed to observe and analyze the effect of the variation in scale parameter (c) of Weibull PDF on different costs of wind power for a constant schedule power. The shape parameter of the two WPGs is also kept constant at $k = 2$. According to [30], the capacity factor of a particular WPG has a value in a range from 30% to 45% of their installed capacity, thus the two WPGs are assumed to have fixed schedule powers at 25 MW and 20 MW, respectively. The cost coefficients of the two WPGs are kept with the same values used in Case 1. The impact of variation of the Weibull scale parameter of WPG1 and WPG2 on the different types of costs is demonstrated in Figures 13 and 14, respectively.

The total generation cost of wind power reached its minimum value at a scale parameter value that lies in the middle of the selected range. With increasing the value of

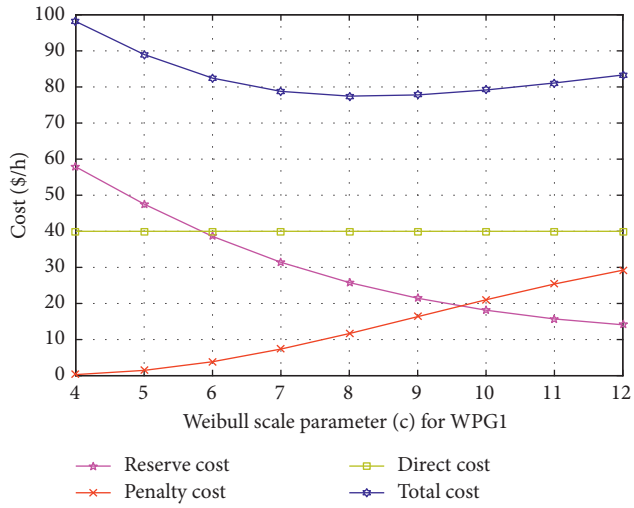

Figure 13: Impact of scale (c) variation for WPG1 on different wind power costs.

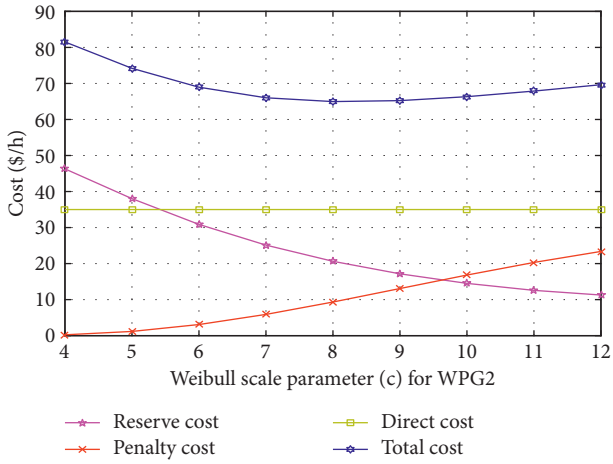

Figure 14: Impact of scale (c) variation for WPG2 on different wind power costs.

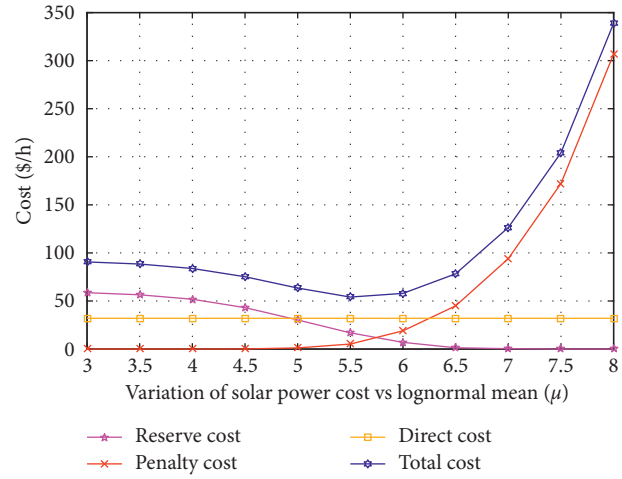

Figure 15: Impact of lognormal mean (μ) variation for SPV on different solar power costs.

scale parameter and keeping the scheduled power constant, higher wind speeds with certain probabilities dominate and the penalty cost rises which causes a rise in the overall generation cost. On the other hand, the reserve cost decreases slightly after a specific scale parameter value.

For studying the effect of changing the lognormal PDF mean parameter (μ) on the cost of solar power, μ is varied in a range from 3 to 8 with an increase of 0.5. The scheduled power of SPG is fixed at 20 MW and the standard deviation (σ) is 0.6. The coefficients of power cost related to the SPG do not differ from those used in Case 1. Figure 15 presents the curves of cost relevant to the solar output power. It is noticed from this figure that the total solar output power cost reduces gradually until reaching the minimum total cost at $\mu = 5.5$. The penalty and reserve costs are the same at around $\mu = 5.8$. After that, a sharp increase in the penalty cost happens, causing a sudden increase in the total solar power cost. Solar irradiance (I) is extremely sensitive to μ value, and accordingly the solar output power.

If μ has a low value, solar irradiance will be low and as a result, the output power will also be low, so almost all reserve power will be crucial to compensate this shortage. In contrast, if μ has a high value, irradiance (I) will have a higher value, and accordingly, the output power of the SPG tends to be higher.

6.5. Case 5: Minimization of Total Generation Cost for the Modified IEEE-57 Bus Power System. In this case, the IEEE-57 bus system has been modified through replacing the two TPGs connected at bus 2 and bus 6 with two WPGs. In addition to that, the TPG connected at bus 9 is replaced by a SPG. This case has been implemented to verify the validity of MPA in solving more complicated power systems. The active and reactive components of load demand of this system are 1250.8 MW and 336.4 MVAR, respectively, at base of 100 MVA. Table 8 shows the main characteristics of the IEEE 57 bus system. The objective function and system constraints are the same as in equations (8)–(17). To verify the results

Table 8: Summary of the modified IEEE-57 bus power system.

Item	Number	Details
Buses	57	[12]
Branches	80	[12]
TPGs	4	Linked at bus 1 (swing), bus 3, bus 8, and bus 12
WPGs	2	Linked at bus 2 and bus 6
SPG	1	Linked at bus 9
Control variables	13	The scheduled power output from: TPG2, TPG3, TPG4, WPG1, WPG2 and SPG, generator buses voltages (7 generators)
System load	—	1250.8 MW, 336.4 MVAr
Permissible load buses voltage range	50	[0.94–1.06] p.u.

Table 9: OPF simulation results-case 5- IEEE-57 bus system.

	Min	Max	MPA	GA
Control variables				
P_{TG1} (MW)	0	576	99.9914	188.4596
P_{TG2} (MW)	40	140	116.066	56.5657
P_{TG3} (MW)	100	550	335.5273	317.3665
P_{TG4} (MW)	100	410	409.9677	401.6186
$P_{wdsch,1}$ (MW)	30	100	100	100
$P_{wdsch,2}$ (MW)	30	100	99.9999	99.9999
P_{slsch} (MW)	30	100	100	100
V_1 (p.u.)	0.95	1.1	1.071359	1.061775
V_2 (p.u.)	0.95	1.1	1.070425	1.052108
V_3 (p.u.)	0.95	1.1	1.065195	1.037525
V_6 (p.u.)	0.95	1.1	1.063282	1.054972
V_8 (p.u.)	0.95	1.1	1.073292	1.051139
V_9 (p.u.)	0.95	1.1	1.053422	1.030074
V_{12} (p.u.)	0.95	1.1	1.059021	1.039221
Parameters				
Q_{TG1} (MVAr)	−140	200	47.8601	86.31078
Q_{TG2} (MVAr)	−10	60	28.9186	8.0839
Q_{TG3} (MVAr)	−140	200	51.0596	29.3683
Q_{TG4} (MVAr)	−150	155	50.3662	50.109
$Q_{wdsch,1}$ (MVAr)	−17	50	49.9642	27.8327
$Q_{wdsch,2}$ (MVAr)	−8	25	−7.7166	16.9735
Q_{slsch} (MVAr)	−3	9	8.94297	8.9991
Total generation cost ($/h)			**20234.39**	20300.7093
P_{loss} (MW)			10.7522	13.2098
V_d (p.u.)			1.4972	1.3837

obtained by MPA, GA is used to solve the OPF problem under the same conditions. The two algorithms have been run for 10 times with a maximum of 500 iterations for each run as the criteria of ending the run. The obtained results show the effectiveness of MPA in terms of minimizing total generation cost maintain the system constraints within the predefined settings as shown in Table 9 and Figure 16. The statistical details values of total generation cost with maximum, minimum, mean, and standard deviation over 10 runs of each algorithm are recorded in Table 10, while the convergences of MPA and other algorithms are provided in Figure 17.

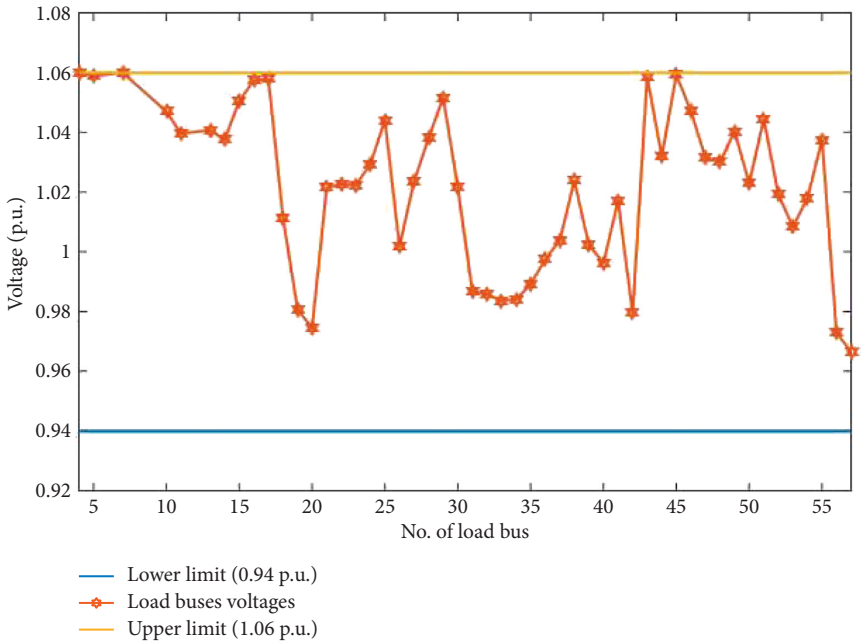

Figure 16: Voltages profile of load buses-case 5.

Table 10: Statistical details values of total generation cost ($/h)-case 5.

Algorithm	Max.	Min.	Mean	Std dev
MPA	20240.27	**20234.39**	20236.97	**1.96**
GA	20416.086	20300.71	20338.85	33.76

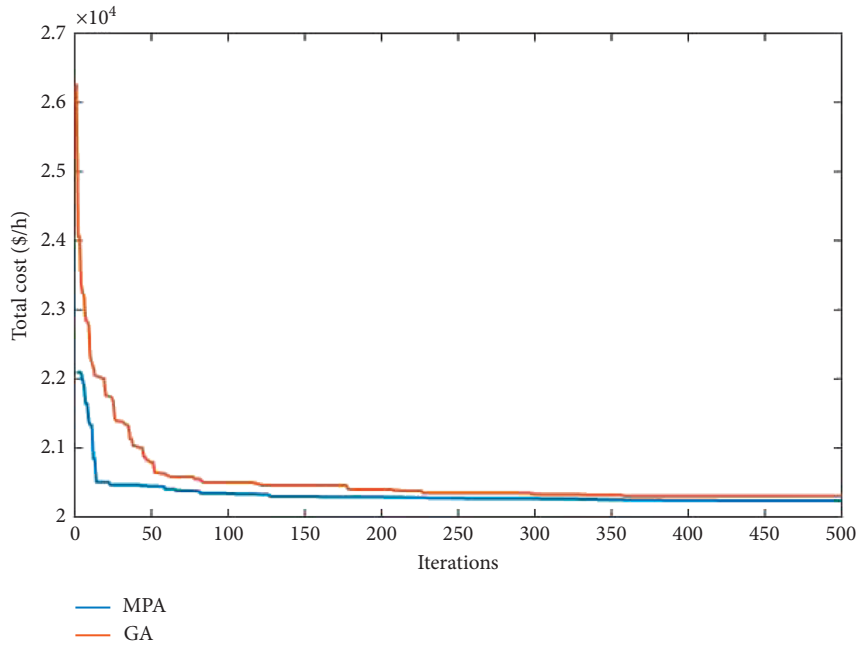

Figure 17: Convergence characteristics-case 5.

7. Conclusions

In this paper, a new application of the marine predator algorithm (MPA) is proposed for solving the OPF problem for IEEE-30 bus and IEEE-57 bus power systems that have been modified to include wind and solar photovoltaic energy sources in addition to the thermal generators. The stochastic nature of renewable energy sources has been modeled in this paper based on the Weibull and lognormal PDFs. The simulation results of MPA under various case studies have been compared with the results obtained by some recent optimization algorithms such as PSO, MPSO, and GA, in addition to the results of SHADE-SF provided in the literature. The simulation results prove the MPA effectiveness among the other algorithms in terms of minimizing the total generation cost. The impact of changing the penalty and reserve cost coefficients of WPGs and SPG is also studied due to their direct impact on the optimal scheduled active powers and their corresponding generation costs. The simulation results show also that the values of the Weibull PDF scale parameter (c) and lognormal PDF mean parameter (μ) have to be carefully defined as they have a direct effect on the different costs of wind and solar powers.

Data Availability

For the data-related issue, kindly contact skamel@aswu.edu.eg

Conflicts of Interest

The authors declare that they have no conflicts of interest.

Acknowledgments

The authors thank the support of the National Research and Development Agency of Chile (ANID), ANID/Fondap/15110019.

References

[1] J. Carpentier, "Contribution to the economic dispatch problem," *Bulletin of Social Francoise Electriciens*, vol. 8, no. 3, pp. 431–447, 1962.

[2] H. Hua Wei, H. Sasaki, J. Kubokawa, and R. Yokoyama, "An interior point nonlinear programming for optimal power flow problems with a novel data structure," *IEEE Transactions on Power Systems*, vol. 13, no. 3, pp. 870–877, 1998.

[3] A. A. M. Al-Qaness, A. A. Ewees, H. Fan, L. Abualigah, and M. A. Elaziz, "Marine predators algorithm for forecasting confirmed cases of COVID-19 in Italy, USA, Iran and Korea," *International Journal of Environmental Research and Public Health*, vol. 17, pp. 1–14, 2020.

[4] M. A. Soliman, H. M. Hasanien, and A. Alkuhayli, "Marine predators algorithm for parameters identication of triple-diode photovoltaic models," *IEEE Access*, vol. 8, pp. 155832–155842, 2020.

[5] J. B. Park, Y. W. Jeong, J. R. Shin, and K. Y. Lee, "An improved particle swarm optimization for nonconvex economic dispatch problems," *IEEE Transactions on Power Systems*, vol. 25, no. 1, pp. 156–166, 2009.

[6] D. Tian and Z. Shi, "MPSO: modified particle swarm optimization and its applications," *Swarm and Evolutionary Computation*, vol. 41, pp. 49–68, 2018.

[7] A. G. Bakirtzis, P. N. Biskas, C. E. Zoumas, and V. Petridis, "Optimal power flow by enhanced genetic algorithm," *IEEE Transactions on Power Systems*, vol. 17, no. 2, pp. 229–236, 2002.

[8] P. P. Biswas, P. N. Suganthan, and G. A. J. Amaratunga, "Optimal power flow solutions incorporating stochastic wind and solar power," *Energy Conversion and Management*, vol. 148, pp. 1194–1207, 2017.

[9] S. A. Sadat and M. Sahraei-Ardakani, "Customized sequential quadratic programming for solving large-scale AC optimal power flow," in *Proceedings of the 2021 North American Power Symposium (NAPS)*, pp. 1–6, IEEE, Texas A&M University, College Station, TX, USA, November 2021.

[10] M. H. Nadimi-Shahraki, S. Taghian, S. Mirjalili, L. Abualigah, M. Abd Elaziz, and D. Oliva, "EWOA-OPF: effective whale optimization algorithm to solve optimal power flow problem," *Electronics*, vol. 10, no. 23, p. 2975, 2021.

[11] E. Naderi, M. Pourakbari-Kasmaei, F. V. Cerna, and M. Lehtonen, "A novel hybrid self-adaptive heuristic algorithm to handle single- and multi-objective optimal power flow problems," *International Journal of Electrical Power & Energy Systems*, vol. 125, Article ID 106492, 2021.

[12] M. A. Taher, S. Kamel, F. Jurado, and M. Ebeed, "Modified grasshopper optimization framework for optimal power flow solution," *Electrical Engineering*, vol. 101, no. 1, pp. 121–148, 2019.

[13] M. H. Nadimi-Shahraki, S. Taghian, and S. Mirjalili, "An improved grey wolf optimizer for solving engineering problems," *Expert Systems with Applications*, vol. 166, Article ID 113917, 2021.

[14] K. Nusair and F. Alasali, "Optimal power flow management system for a power network with stochastic renewable energy resources using golden ratio optimization method," *Energies*, vol. 13, no. 14, p. 3671, 2020.

[15] I. U. Khan, N. Javaid, K. A. A. Gamage, C. J. Taylor, S. Baig, and X. Ma, "Heuristic algorithm based optimal power flow model incorporating stochastic renewable energy sources," *IEEE Access*, vol. 8, pp. 148622–148643, 2020.

[16] F. Alasali, K. Nusair, A. M. Obeidat, H. Foudeh, and W. Holderbaum, "An analysis of optimal power flow strategies for a power network incorporating stochastic renewable energy resources," *International Transactions on Electrical Energy Systems*, vol. 31, no. 11, Article ID e13060, 2021.

[17] M. Abdullah, N. Javaid, I. U. Khan, Z. A. Khan, A. Chand, and N. Ahmad, "Optimal power flow with uncertain renewable energy sources using flower pollination algorithm," in *Proceedings of the International Conference on Advanced Information Networking and Applications*, pp. 95–107, Springer, Cham, Switzerland, March 2019, Advanced Information Networking and Applications.

[18] M. J. Laly, E. P. Cheriyan, and A. T. Mathew, "Particle swarm optimization based optimal power flow management of power grid with renewable energy sources and storage," in *Proceedings of the 2016 Biennial International Conference on Power and Energy Systems: Towards Sustainable Energy (PESTSE)*, pp. 1–6, IEEE, Bengaluru, India, January 2016.

[19] A. E. Chaib, H. R. E. H. Bouchekara, R. Mehasni, and M. A. Abido, "Optimal power flow with emission and non-smooth cost functions using backtracking search optimization algorithm," *International Journal of Electrical Power & Energy Systems*, vol. 81, pp. 64–77, 2016.

[20] R. D. Zimmerman, C. E. Murillo-Sánchez, and R. J. Thomas, "Matpower," http://www.pserc.cornell.edu/matpower.
[21] A. Panda and M. Tripathy, "Security constrained optimal power flow solution of wind-thermal generation system using modified bacteria foraging algorithm," *Energy*, vol. 93, pp. 816–827, 2015.
[22] L. Shi, C. Wang, L. Yao, Y. Ni, and M. Bazargan, "Optimal power flow solution incorporating wind power," *IEEE Systems Journal*, vol. 6, no. 2, pp. 233–241, 2012.
[23] C. Tian-Pau, "Investigation on frequency distribution of global radiation using different probability density functions," *International Journal of Applied Science and Engineering*, vol. 8, no. 2, pp. 99–107, 2010.
[24] H. M. Dubey, M. Pandit, and B. K. Panigrahi, "Hybrid flower pollination algorithm with time-varying fuzzy selection mechanism for wind integrated multi-objective dynamic economic dispatch," *Renewable Energy*, vol. 83, pp. 188–202, 2015.
[25] S. Surender Reddy, P. R. Bijwe, and A. R. Abhyankar, "Real-time economic dispatch considering renewable power generation variability and uncertainty over scheduling period," *IEEE Systems Journal*, vol. 9, no. 4, pp. 1440–1451, 2015.
[26] A. Faramarzi, M. Heidarinejad, S. Mirjalili, and A. Gandomic, "Marine predators algorithm: a nature-inspired meta-heuristic," *Expert Systems with Applications*, vol. 152, pp. 1–10, 2020.
[27] M. Abdel-Basset, R. Mohamed, M. Elhoseny, R. K. Chakrabortty, and M. Ryan, "A hybrid COVID-19 detection model using an improved marine predators algorithm and a ranking-based diversity reduction strategy," *IEEE Access*, vol. 8, pp. 79521–79540, 2020.
[28] A. Qamar, Y. Irfan, and S. Mehreen, "Political optimizer: a novel socio-inspired meta-heuristic for global optimization," *Knowledge-Based Systems*, vol. 195, pp. 1–30, 2020.
[29] O. Alsac and B. Stott, "Optimal load flow with steady-state security," *IEEE Transactions on Power Apparatus and Systems*, vol. PAS-93, no. 3, pp. 745–751, 1974.
[30] B. Veatch, "Cost and performance data for power generation technologies," *Prepared Nat Renew Energy Laboratory*, 2012.